Process Safety and Environmental Protection 217 (2026) 109371

Contents lists available at ScienceDirect

Process Safety and Environmental Protection

journal homepage: www.journals.elsevier.com/process-safety-and-environmental-protection

Investigation of the particle separation characteristics in the submicron and nanoscale size range for cake-forming surface filter media in gas cleaning applications

Peter Bächler [a,*], Felizia Zhang [a], Jörg Meyer [a], Qian Zhang [b], Achim Dittler [a]

[a] Institute of Mechanical Process Engineering and Mechanics, Karlsruhe Institute of Technology, Straße am Forum 8, Karlsruhe 76131, Germany
[b] Institute of Particle Technology, University of Wuppertal, Gaußstraße 20, Wuppertal 42119, Germany

ARTICLE INFO

Keywords:
Nanoparticle emissions
Surface filters
Pulse-jet cleaned filters
Baghouse filters
Filtration
Gas cleaning
Aerosol measurement

ABSTRACT

Current industrial dust emission limits and emission characterization in filter testing standards for cleanable surface filters are based on gravimetric (non-size-resolved) measurements. However, submicron and nanoscale particles often dominate emissions in terms of particle number concentration. This study provides a comprehensive analysis of the fractional separation efficiency and its evolution during dust cake formation over the full emission-relevant size range. Experiments were conducted in a filter test rig for cleanable filter media (VDI 3926 / DIN ISO 11057). Because particle penetration decreases rapidly as the dust cake is formed, a suitable experimental methodology was developed. Fractional separation efficiency was measured using submicron test aerosols (dried NaCl and high-purity water) that do not contribute to cake formation or enhance filtration characteristics. Between these measurements, a separate phase using coarse test dust (Pural SB) enabled controlled cake formation, while concentration decay on the clean-gas side was monitored. Aerosol measurements covered a wide range from approximately 10 nm to 10 μm using a combination of light-scattering aerosol spectrometer, condensation particle counter, and scanning mobility particle sizer. The filter medium itself had a most penetrating particle size (MPPS) of 305 nm with an efficiency of 53.3% and an upper separation limit near 4 μm. Even small increases in differential pressure (e.g. from 100 Pa to 200 Pa) shifted the emission-relevant range completely into the submicron particle size range. At 500 Pa, efficiency reached 99.8% at a MPPS of 126 nm. The results demonstrate the particle-size dependent filtration kinetics and the mitigation potential of surface filters considering potential (ultra-) fine particle emissions.

1. Introduction

The most prominent technology for particle separation for industrial gas-cleaning applications are pulse-jet cleaned filters. Within the scope of the WGC-BREF a new range for gravimetrical dust concentration limits for processes where fabric filters can be applied is specified between 1–5 mg/m^3 (European Commission, 2023).

The exact limit depends on the decision of public authorities based on the individual application. The gravimetrical determination of an average total (and thus non-size-resolved) dust emission is also considered in testing standards (such as e.g. VDI 3926 or DIN ISO 11057) for surface filter media, where the mass difference of an absolute filter is evaluated before and after a filter test procedure consisting of multiple filtration cycles (DIN ISO 11057, 2011; VDI 3926, 2004).

At the beginning of an individual filtration cycle particles can penetrate straight through the filter medium to the clean gas side. With increasing cake thickness particle penetration decreases down to a "zero" level due to enhanced separation capabilities of the dust layer (Binnig et al., 2009). When a cleaning criterion is met (e.g. after a fixed time interval or after exceeding a maximum differential pressure), the filter is regenerated and the dust cake is removed (e.g. via jet-pulse cleaning) enabling renewed particle penetration. This transient particle emission behavior is not considered within the determination of average gravimetrical particle concentrations.

In the industrial application, where e.g. defects or seams of the filter element or leaks can enable particle bypass (Bach and Schmidt, 2007, Lacerda et al., 2022, Li et al., 2022), gravimetrical measurements might be a suitable metric. Here, a potential exceedance of dust emission limits can be the result of leaks or unsuitable operating conditions of the

* Corresponding author.
E-mail address: peter.baechler@kit.edu (P. Bächler).

https://doi.org/10.1016/j.psep.2026.109371
Received 7 April 2026; Received in revised form 17 July 2026; Accepted 28 July 2026
Available online 29 July 2026

Symbols and abbreviations

Symbol, Unit, Definition

A_{filter}	m^2, Filter area
a	-, Empirical constant a > 0
b	-, Empirical constant b > 0
C_1	-, Constant $C_1 = e^{-\eta_{FM}(x) \bullet f_{FM}}$
C_2	-, Constant $C_2 = -\eta_{FM}(x) \bullet f_{FM}$
$C_{n,clean-gas}(x)$	cm^{-3}, Particle number concentration on the clean-gas side
$C_{n,raw-gas}(x)$	cm^{-3}, Particle number concentration on the raw-gas side
c_0	s^{-1}, Constant parameter for the given filtration conditions and particle properties
$f_{DC}(t)$	-, Structural parameter of the dust cake at the filtration time t
f_{FM}	-, Structural parameter of the filter medium
Δm	g, Mass difference / separated dust mass on the filter medium
$P(x)$	-, Penetration efficiency of particles of size x
Δp	Pa, Differential pressure
Δp_0	Pa, Residual differential pressure
$\dot{V}$	m^3 /s, Volume flow
W	g/m^2, Dust area load
w_{filter}	cm/s, Filter face velocity
$T(x)$	-, Fractional separation efficiency
t	s, Filtration time
Δt	s, Time interval
x	m, Particle size (e.g. electrical mobility or optical particle diameter)
x_{MPPS}/MPPS	m, Most penetrating particle size
$\eta_D(x)$	-, Single fiber collection efficiency for particles of size x based on the diffusion mechanism
$\eta_{DC}(x)$	-, Single fiber collection efficiency for particles of size x for the dust cake
$\eta_{FM}(x)$	-, Single fiber collection efficiency for particles of size x for the filter medium
$\eta_I(x)$	-, Single fiber collection efficiency for particles of size x based on the interception mechanism

baghouse filter that leads to the penetration of (significant amounts) of larger particles to the clean-gas side resulting in high gravimetrical concentrations (Bächler et al., 2023, Kurtz et al., 2017). In this context Steiner and Lanzerstorfer (2024) discussed measurement uncertainty issues that can arise for low dust mass concentrations on the clean gas side of baghouse filters (i.e. in case of leak-free operation and suitable operating conditions) for certain measurement systems.

The fractional separation efficiency curve of typical filter media (including both surface and depth filters) spans a size range down into the nanometer region that is often neglected in the context of cleanable surface filters. Two exceptions include studies from Simon et al. (2014) and Lacerda et al. (2022) that report fractional separation efficiencies of surface filter media – however only the filter material was analyzed and the evolution of the fractional separation efficiency during filter operation was not considered / the focus of the studies. Simon et al. (2014) report fractional separation efficiencies for two filter media (acrylic polymer microporous coating over a polyester needle-felt medium: approx. 30% efficiency at MPPS of 200 nm; non-woven polyester medium with an anti-clogging thermo-bonded surface: approx. 20% minimum efficiency at MPPS of 350 nm). Lacerda et al. (2022) report minimum efficiencies of above 90% at a MPPS below 100 nm for a membrane surface filter medium. Due to the high relevance of submicron particles in filtration applications, particle number based measurements have long been established e.g. for the characterization of the performance of depth filters (DIN EN ISO 16890, 2016) or engine exhausts (European Commission, 2020).

The contribution of particles in the submicron or nanometer size range to gravimetrical concentrations is rather low and few larger particles (e.g. $x >> 1$ µm) can potentially dominate the total mass based particle emission. There is a dissonance between the actual penetration/emission-relevant particle sizes that are better represented by number based measurements and the actual determination of particle emissions for surface filters that is based on gravimetrical measurements. There are a variety of studies investigating the (transient and size-resolved) particle emission behavior of surface filters using aerosol spectrometers (OPC) – however these studies are limited regarding the lower detectable size range of the measurement technology (approx. 200 nm) (e.g. Binnig et al., 2009; Kurtz et al., 2016; Ding et al., 2025).

The revision of the EU Ambient Air Quality Directive includes a monitoring obligation for ultrafine particles within the scope of ambient air quality monitoring, thus the emission of nanosized particles from technical processes and their mitigation are gaining relevance (European Union, 2024). Without proper characterization methods that take the characteristic transient particle emission behavior of cake-forming surface filters into account, the actual nanoparticle emission, respectively the separation capabilities in the nanoscale region remain unknown.

While there are several studies that investigated nanoscale particle emissions of processes where pulse-jet cleaned surface filters were applied for gas cleaning, no systematic investigation of the separation characteristics in the entire penetration-relevant size range was performed.

Khirouni et al. (2020) investigated the filtration performance of cleanable filters challenged with metallic nanoparticles, where clogging of the filter elements (and thus unstable operation) is a risk. Schiller and Schmid (2015) investigated a filtration process using pre-coat material to protect the filter element and measured very high separation efficiencies. Here, the transient behavior was not taken into account. Boudhan et al. (2018) reported the evolution of the fractional separation efficiency with increasing differential pressure (cake formation) for a filter element. While the transient behavior was not directly taken into account by the measurements, a very slow cake formation over multiple minutes presumably enabled a sufficiently accurate characterization. The used test aerosol was very constricted in its size range so that no complete characterization of the separation characteristics was performed. Leung and Choy (2018) investigated the separation efficiency and its evolution under nano-aerosol loading by resorting to a single particle size of 300 nm (and thus not considering the complete penetration range) for a filter efficiency determination.

In a previous study, the filtration kinetics (evolution of the fractional separation efficiency with ongoing cake formation) was investigated where OPC measurements demonstrated how different particle sizes show a varying decay behavior, indicating a significant change in fractional separation efficiency and most penetrating particle size over the course of a filtration cycle (Zhang, 2022). In another study, the transient nanoscale particle emission behavior was investigated for a biomass power plant equipped with pulse-jet cleaned filters where cake formation caused a fast concentration decay on the clean-gas side and the size distribution of the particle emission had to be determined using a special methodology and combination of multiple aerosol measurement devices (OPC, CPC and SMPS system) (Bächler et al., 2024). While the test aerosol was also constricted in its size range (similar to Boudhan et al., 2018) the study demonstrated the relevance of nanoscale particle emissions for processes where pulse-jet cleaned filters are applied.

In this article, an experimental methodology is proposed that enables the characterization of the fractional separation efficiency and its evolution with ongoing cake formation for surface filter media in gas cleaning applications.

1.1. Preliminary considerations for the experimental investigation of the evolution of the fractional separation efficiency for cake-forming surface filters

Several conditions have to be met in order to correctly determine the fractional separation efficiency for surface filters and its evolution with proceeding cake formation, due to the characteristic particle emission behavior of the filters.

To gain information on the complete emission-relevant size-range a test aerosol with a wide size distribution across (or exceeding) the entire size range of the fractional separation efficiency curve has to be generated. Here, for depth filters typical test aerosols include DEHS, or salt aerosols (e.g. KCL or NaCl aerosols).

The corresponding aerosol measurement technology to determine the fractional separation efficiency in turn also has to cover this emission-relevant particle size range and offer a sufficient temporal resolution (e.g. 1 Hz) to cover the dynamic behavior of particle emission peaks (up to several tens of thousands particles per cubic centimeter) down to a "zero" concentration level.

Diffusion charge-based devices that can only measure down to a non-zero "background level" (especially in the lower size classes) are not as suitable for this purpose (Bächler et al., 2022), even though the temporal resolution would be sufficient.

Light-scattering aerosol spectrometers (OPC), though they are limited by the lower detectable size limit of approx. 200 nm (optical particle size) are generally suitable for the determination of the temporally and size-resolved particle concentrations for this application (Zhang, 2022). Especially in research setups and filter testing these devices are established to gain additional insights on the penetration and emission characteristics of the corresponding filter media, especially when resorting to fine dust fractions such as the $PM_{2.5}$-fraction (Bächler et al., 2026; Binnig et al., 2009; Bach and Schmidt, 2007; Lacerda et al., 2022; Li et al., 2022; Knisley et al., 2026; Höflinger, 2025; Bächler et al., 2022).

Condensation particle counters (CPC) offer concentration measurements with sufficient temporal resolution that also cover the relevant concentration range, but offer no size-resolved information. They are suitable as a tracer for the total (mostly submicron / nanoscale) particle emission that is dominated by particle number.

CPCs in combination with a differential mobility analyzer (DMA) enable the measurement of size resolved particle concentrations (SMPS-system) down to the nanometer range (electrical mobility diameter) (Bächler et al., 2024). When working with SMPS-systems, particle concentrations should remain constant during the measurement duration in order to minimize measurement errors. For surface filters, the particle concentration on the clean-gas side decreases over time due to the formation of the dust cake. Depending on the filter medium and raw-gas concentration, there may be only a limited timeframe where sufficient concentrations can be detected in a corresponding size class before the concentration decreases down to zero. However, the scan of a size distribution may take up to several minutes dependent on the individual operation settings of the SMPS (e.g. size range). Therefore, within the context of a quickly decaying particle concentration, the concentrations of particle sizes that are measured at a later stage during the scanning procedure are underestimated. This issue has been addresses in a past publication, where SMPS-scans were corrected based on the particle concentration decay (total non-size resolved concentration) on the clean gas side (Bächler et al., 2024). The corresponding size range of the combustion aerosol on the raw-gas side spanned a size range of 30 – 350 nm (mode: 121.9 nm). Such a correction was only valid since in that case the overall concentration decay was mostly uniform among all size classes. This does not necessarily have to be valid for all operating conditions and types of dusts (Zhang, 2022).

Summarizing, a combination of the aforementioned aerosol measurement devices (OPC, CPC and SMPS) is capable to cover a total size range of approx. 10 nm up to 10 μm and offers a sufficient concentration range and temporal resolution (with the exception of the SMPS-system that relies on longer measurement periods). While these devices are often conjointly applied in filter testing for depth filter media, systematic measurements have (to the author's knowledge) not been performed for cleanable surface filter media taking into account cake formation.

A suitable measurement methodology could work around the issue of particle concentration decay that can affect SMPS measurements by stopping the dust feeder for the main/primary test dust for cake formation (here: periodical dosage of mostly supermicron test dust) and implementing a dedicated measurement-phase for the determination of the fractional separation efficiency. The corresponding test aerosol for this measurement phase must not affect the filtration performance (e.g. contribute to cake formation) within the scanning procedure of an SMPS.

2. Experimental set-up, materials and methods

2.1. Filter test rig

The filter test rig used for the experimental investigation was a typical test rig for the characterization and comparison of surface filter media based on (VDI 3926, 2004) respectively (DIN ISO 11057, 2011). Several modifications were made to the standard setup which are displayed in Fig. 1.

Two different possibilities for aerosol generation were applied in this study. Test dust can be dispersed directly into the raw-gas duct (no sampling lines) with a (rotating-brush) dust feeder. Furthermore, two aerosol generators from liquid solutions (AGK 2000 from Palas® and ATM 221 from Topas®) enable the generation of a submicron and nanoscale aerosol (compare 2.3). In 2.5 the experimental methodology is described whereby the different types of aerosol generators are used in an alternating fashion.

After dispersion into the raw-gas duct the aerosol is neutralized by a Kr_{85} radioactive source. The total volume flow is split into two parts, whereby one part (50 l/min) is discarded and led over an absolute filter and subsequently into the environment. The remaining volume flow including potential sample flows of the aerosol measurement devices (total of 35 l/min to adjust a filter face velocity of approx. 2.3 m/min) is sucked through the filter medium at a 90° angle. It cannot be ruled out that coarser particle sizes of the test dust can not follow this flow profile

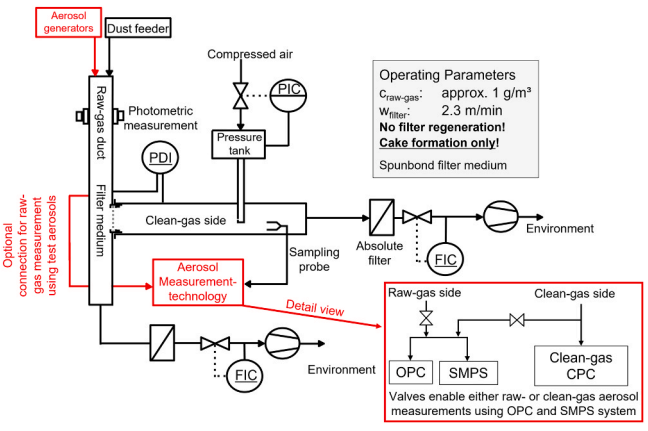

Fig. 1. Filter test rig adapted from VDI 3926 (or DIN ISO 11057) and corresponding modifications for the systematic investigation of the separation characteristics across a wide particle size range for cake-forming surface filters.

due to inertia. However, raw-gas concentration is determined gravimetrically in preliminary experiments by determining the mass difference of the filter before and after dust loading in a certain time interval for a given volume flow according to Equation 1. As such only particles that are transported to the filter medium are taken into account for the gravimetrical raw-gas concentration.

$$c_{raw-gas} = \frac{\Delta m}{\dot{V} \bullet \Delta t} = \frac{\Delta m}{w_{filter} \bullet A_{filter} \bullet \Delta t} \quad \text{Eq. 1}$$

A photometric measurement monitors the dust concentration and is calibrated against the gravimetrically determined raw-gas concentrations (approx. 1 g/m³ in this study). From the raw-gas concentration and the photometric measurement the dust area load on the filter medium after cake formation can be calculated according to Equation 2.

$$W = \frac{\Delta m}{A_{filter}} = c_{raw-gas} \bullet w_{filter} \bullet \Delta t \quad \text{Eq. 2}$$

The filter medium is a circular filter coupon installed within a filter holder and separates the raw-gas duct and the clean gas side. The differential pressure between raw- and clean-gas side is measured with a differential pressure transmitter (DS−010, Kalinsiky Sensor Elektronik GmbH & Co. KG). The linear increase of differential pressure during cake formation serves as further indication for the separated dust mass / dust area load and a constant feed-rate of the dust feeder. The regeneration equipment (e.g. pressure vessel, etc.) was not used for this investigation (cake formation only).

Further modifications to the standard setup include sophisticated aerosol measurement technology. In the standard setup according to VDI 3926 or DIN ISO 11057 only a gravimetrical measurement of the (average) total dust emission is mandatory. In this investigation no gravimetrical measurement was performed, as advanced aerosol measurement technology is necessary to investigate the submicron and nanoscale particle emission.

2.2. Aerosol measurement technology

In this study a measurement system consisting of a condensation particle counter (TSI® CPC 3775), an aerosol spectrometer (Palas® Promo®2000 with welas®2100 sensor) and an SMPS-system (TSI® Electrostatic Classifier Model 3082 with Advanced Aerosol Neutralizer 3088, Long DMA 3081A00 and CPC 3756) was used to cover a wide particle size and concentration range.

The CPC 3775 was constantly monitoring the total particle concentration on the clean gas side (4 nm up to < 3 µm) while the OPC (size range of approx. 200 nm up to 10 µm) and SMPS-system (size range of approx. 15 nm – 600 nm) were both connected to an adjustable sampling line that could be either connected to the raw-gas side or the clean-gas side. That way the determination of raw- and clean-gas size distributions and the calculation of the fractional separation efficiency is possible. The devices are also suitable for the expected particle concentration ranges and characterization of the transient particle emission behavior. In order to enable comparability of the corresponding concentrations and distributions between OPC and SMPS system the concentrations in a corresponding size interval were based on the difference between the decadic logarithm of the upper and lower particle size of the interval. The size resolution of the SMPS-system was 64 size classes / decade and 32 size classes / decade for the aerosol spectrometer (dC_n / $dlog(x)$ = 64 for the SMPS-system, respectively dC_n / $dlog(x)$ = 32 for the OPC at a concentration of dC_n = 1 cm^{-3}). Measurements of particles in the emission-relevant submicron size range do not necessarily rely on isokinetic sampling.

To improve the agreement of the two devices that rely on different measurement principles and allocate particle concentrations to either an electrical mobility particle diameter (SMPS-system) or an optical particle diameter (OPC), a set of measurements to perform a calibration would potentially improve the results. One such way would be to operate the SMPS-system at a constant classifier voltage and compare the measured concentrations of a corresponding aerosol at specific sizes (classifier voltages) using an OPC and CPC. This would make a correction of the optical particle diameter to align with the electrical mobility diameter and a correction of counting efficiency possible.

However, no such calibration was performed in this study due to an overall good agreement between the devices in the overlapping region especially when resorting to the fractional separation efficiency curves that were the focus of this investigation (compare e.g. Sections 2.3 and 2.6).

2.3. Aerosols for filter testing

Two different aerosols were used in the investigation:

- A test aerosol for the determination of the fractional separation efficiency was generated using two different nebulizers. A NaCl aerosol was generated from a Topas ATM 221 (pressure: 2 bar, concentration of the salt solution: 35 g NaCl / l high-purity water) that is especially suitable for the generation of aerosols with comparably low-concentrations. This is necessary since the test aerosol must not contribute to cake formation and improve the separation efficiency of the dust cake during measurement procedures. Furthermore, high-purity water (approx. 7 µS/cm) was dispersed using a Palas® AGK (pressure: 2 bar). Both aerosols were dried after nebulization using diffusion driers and subsequently mixed before entering the raw-gas duct. Thus, only residue ultrafine particles from the high purity water and NaCl particles remain that are suitable for the determination of the fractional separation efficiency in the submicron and nanoscale region.
- The test dust for cake formation was Pural SB [chemical composition AlO(OH) – boehmite] from the manufacturer Sasol Germany GmbH which was dispersed using a rotating brush dust feeder. It has a solid density of 2800 kg/m³ and a mass median diameter of approx. 35 µm (Bächler et al., 2022). SEM images of the test dust can be found in (Kurtz et al., 2017).

In Fig. 2, exemplary size distributions of the NaCl test aerosol (a) and the test dust Pural SB (b) from raw-gas measurements are displayed. There is a good agreement between the particle concentrations and sizes of the OPC and SMPS measurement in case of the NaCl aerosol. For Pural SB there are higher deviations what is linked to different dust properties.

The test aerosol for the determination of the fractional separation efficiency was measured on raw-gas side and clean-gas side for each experiment / measurement phase, so that variations of the size distribution and particle concentrations are considered within the evaluation of the fractional separation efficiency. In case of Pural SB, prolonged raw-gas measurements were not possible and the aforementioned size distribution should merely give an indication on the (submicron) fine-fraction of the (coarse) test dust. Stable dosage of the test dust was ensured by photometric measurements in the raw-gas duct. It has to be assumed that part of the coarse fraction is separated by e.g. the sample tubes during the raw-gas OPC and SMPS measurement in Fig. 2. These particle sizes are not relevant within the scope of the (number-based) particle emission / fractional separation efficiency but significantly contribute to cake formation (compare sect. 2.1). Due to a low availability of particles below 100 nm, it is absolutely necessary to use the NaCl test aerosol to be able to characterize the fractional separation efficiency across the entire emission-relevant size fraction.

During separate measurements, a total background particle number concentration of 30 – 70 cm^{-3} was identified for the filter test rig. For these measurements, a very efficient membrane filter medium with a thick dust-cake (2000 Pa differential pressure) was installed in the test rig (assumption: no particle penetration; $T(x)$ = 1) and the resulting clean gas concentration was measured in case of filtration of the NaCl

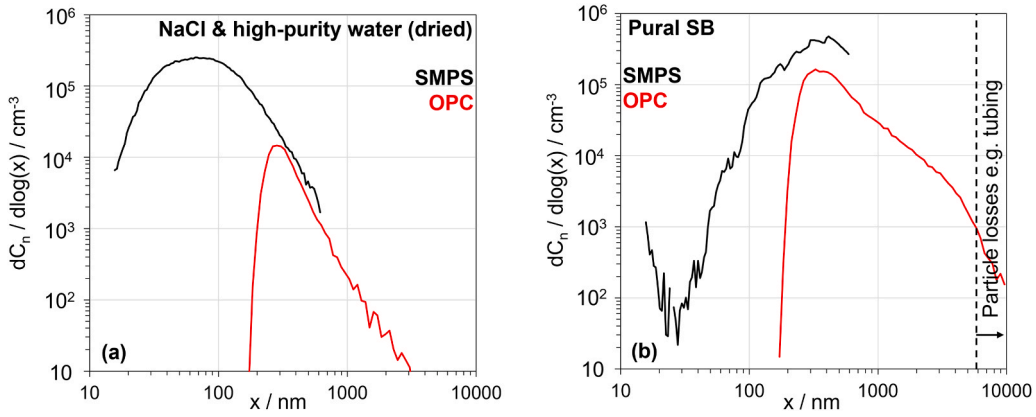

Fig. 2. Particle size distributions and number concentrations of the NaCl test aerosol (a) and test dust Pural SB (b) in their dispersed state in the raw-gas duct.

aerosol. The stated background concentration of 30 – 70 cm^{-3} is a "worst case" estimation not taking possible penetration of NaCl aerosol into account. Few individual particle counts were detected across a size range of approx. 20 – 250 nm for multiple SMPS-scans. The size-resolved raw- and clean-gas concentrations based on particle penetration in this study far exceed the background concentration so that there is no effect on the determined fractional separation efficiencies. The origin of the background concentration is likely based off small leaks that are difficult to completely eliminate for a test rig at this scale.

2.4. Filter medium

The filter medium for the investigation was a spunbond polyester polyamide filter medium (viledon® AT 1285 from the manufacturer Freudenberg Filtration Technologies SE & Co. KG; area weight: 240 g/m^2; thickness: 1 mm; air permeability at 200 Pa: 100 l/dm^2/min) with hydro-entangled microfilaments. The medium has been used in past investigations where it showed increased particle emissions in filter tests (compared to a needle-felt or membrane filter medium) (Bächler et al., 2026). This behavior makes it ideal for this methodical investigation, as comparably long decay periods and high peak concentrations of the emission peaks enable a gradual evaluation of the fractional separation efficiency with proceeding cake formation.

2.5. Experimental methodology for the determination of the fractional separation efficiency

As stated in section 1.1, the determination of the fractional separation efficiency below the detectable size range of the aerosol spectrometer relies on the use of an SMPS-system. Under ideal measurement conditions, the concentration of the aerosol should remain constant during the scanning procedure that takes approx. 1.5 min time for the selected scan settings in this study (size range of approx. 15 nm – 600 nm). The selected size range of the scan enables a sufficient overlap of the detectable size ranges between SMPS-system and OPC (approx. 200 nm – 600 nm). Shorter scan durations would be possible with drawbacks regarding measurement accuracy and the covered size range of the scan. Therefore, measurements during quickly proceeding cake formation should be avoided, as the concentration on the clean gas side may decrease rapidly. The development of a dedicated experimental methodology taking this behavior into account was a key aspect of the investigation.

The evolution of the fractional separation efficiency was gradually determined using multiple filter samples across consecutive experimental runs consisting of three distinct phases as shown in Fig. 3.

– First, the fractional separation efficiency of a new (unloaded) filter sample is determined using the dried NaCl and high-purity water test aerosol. The differential pressure of new samples for the selected filter face velocity of 2.3 m/min is approx. 100 Pa. At least three consecutive scans on the raw-gas side and the clean-gas side are performed by switching the sampling line of OPC and SMPS-system according to the flow-sheet in Fig. 1. Thus, the average concentrations for each size class of the individual measurement device covering the three SMPS-scans or the corresponding measurement period for the OPC (approx. 4.5 min time) could be calculated. From the differential pressure curve, the periods of raw-gas and clean-gas measurements can be easily identified as the volume flow to the

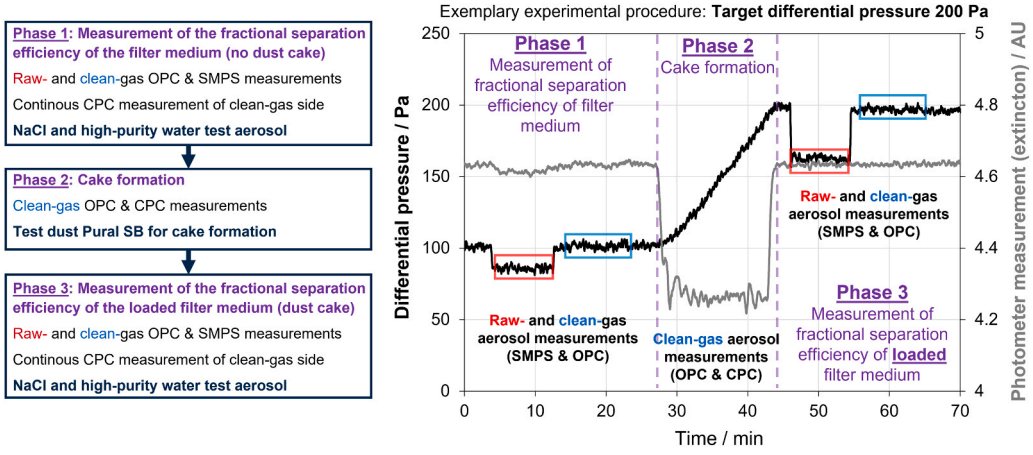

Fig. 3. Experimental methodology for the determination of the fractional separation efficiency and its evolution for cake-forming surface filters.

clean-gas side (and thus the differential pressure across the filter medium) decreases when switching the sampling line from OPC and SMPS-system to the raw-gas side. Aerosol generation was stable and reproducible across the experimental runs, especially when considering the comparably short measurement durations for the characterization of the fractional separation efficiency (compare error bars in Fig. 4). Due to the low mass flow of the test aerosol, the structural properties of the dust cake did not change significantly during the measurement periods according to the constant differential pressure of phase 1 and 3. Further context on aerosol stability can be found in section. 2.7.

– After the initial determination of the fractional separation efficiency, a dust cake is formed under dosage of the test dust Pural SB (nebulizers switched off; no NaCl test aerosol!). During cake formation, the entire aerosol measurement technology is connected to the clean-gas side. This enables the measurement of the particle penetration of the test dust (CPC and OPC measurements) to the clean-gas side (emission peak). The particle emission peak and its decay behavior mainly serve as an indication regarding the comparability of multiple experimental runs. The dust dosage is stopped after reaching a specified differential pressure (respectively dust area load). These target differential pressures were selected based on the penetration behavior (high measurable particle penetration for thin dust cakes) and are rather low compared to typical cleaning differential pressures (e.g. 1000 Pa specified for filter testing according to DIN ISO 11057 or VDI 3926). The measured particle concentration decays for all measurement runs are discussed in section 3.2. After a defined cake formation, a third measurement phase is initiated.
– Measurements of the separation efficiency were repeated after cake formation at the specified differential pressure / dust area load. Again, dried NaCl and high-purity water test aerosol is dispersed into the raw-gas duct and raw- and clean-gas concentrations and size distributions are determined using the OPC and SMPS system (at least three consecutive scans with comparable results). Again, the test aerosol did not contribute to cake formation and modify the separation efficiency, what is the main criterion for the accurate and error-free characterization of the fractional separation efficiency.

2.6. Exemplary results applying the experimental methodology

Fig. 4 highlights the results of an exemplary run (differential pressure level of 200 Pa in phase 3). The average size distributions from 5 consecutive SMPS scans first on the raw-gas side and afterwards on the clean-gas side (duration of 90 s each) are displayed, whereby the error bars indicate the standard deviation between these 5 individual measurements. In case of the OPC, the average distribution for the same time duration is displayed (no error bars – one measurement with longer time duration only). For this measurement duration the particle concentrations for all SMPS scans are very stable. Therefore, structural changes of the filter material or the deposited dust cake that could potentially influence the result of the calculation of the fractional separation efficiency / filtration performance can be ruled out (compare also section 2.7).

The fractional separation efficiency can be calculated according to Equation 3 for both measurement devices using the measured concentrations in a corresponding size class ($dlog(x) = const.$ for each the individual measurement device).

$$T(x) = 1 - \frac{C_{n,clean-gas}(x)}{C_{n,raw-gas}(x)} \quad \text{Eq. 3}$$

When comparing the size distributions and fractional separation efficiencies on the clean-gas side before [(a) and (b)] and after [(c) and (d)] cake formation, a significant improvement can be identified. This behavior corresponds to the decrease in particle penetration during cake formation (compare section 3.2).

OPC and SMPS measurements have an overlapping measurement region from approx. 200 – 600 nm particle size. The counting efficiency of the OPC drops significantly for sizes smaller than 200 nm. The combination of both devices enables the construction of the fractional separation efficiency curve across the (almost) complete emission-relevant

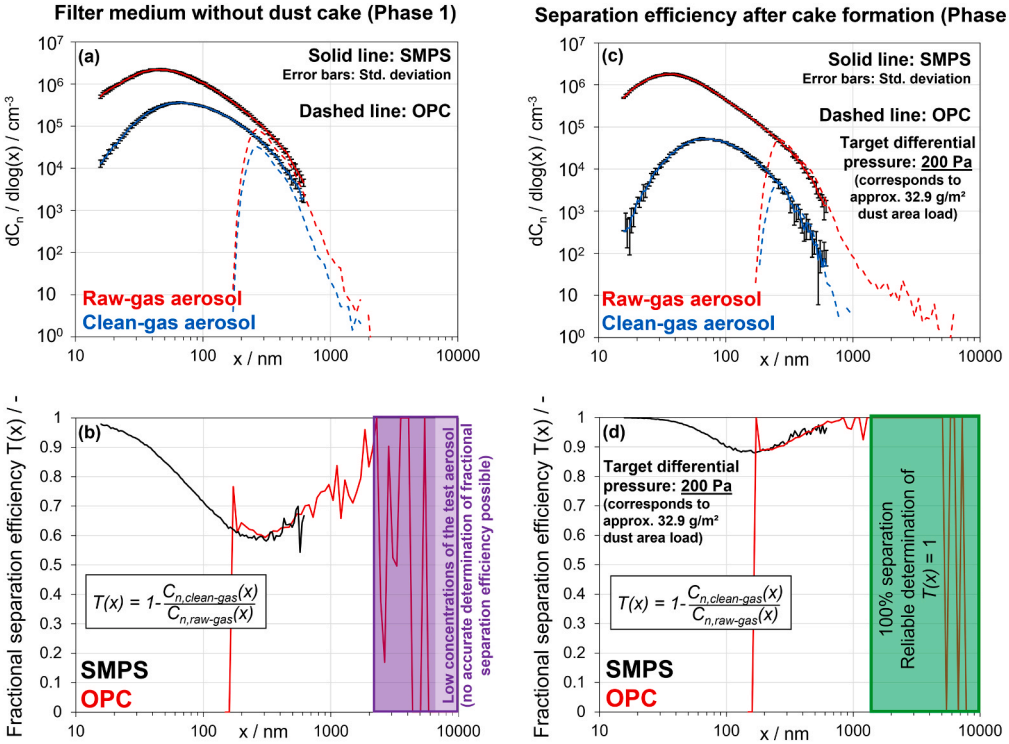

Fig. 4. Results from an experimental run regarding particle size distributions on raw- and clean gas side for phase 1 (a) and 3 (c) and resulting fractional separation efficiencies for phase 1 (b) and 3 (d).

size range. There is a very good agreement between the measured concentrations / fractional separation efficiencies and allocated equivalent particle diameters of OPC and SMPS-system in the overlapping region.

In case of the measurements without dust cake (a) there are minor deviations of the concentrations of OPC and SMPS-system at a specific particle diameter in the overlapping region. Here a calibration (compare section 2.2.) would improve the result. However, in direct comparison with the measurement after cake formation (c) performing the exact same calibration would cause disagreement between the two curves. In that case, without any calibration, the corresponding concentrations in the overlapping region are already nearly identical (e.g. phase 3).

Further calculating the fractional separation efficiencies from the measured concentrations shows that the ratio between raw- and clean-gas concentration yields the same result for both measurement devices for a given particle diameter [(b) and (d)], even when considering the smaller deviations in the aforementioned measured absolute concentrations for the results in phase 1 (a).

For the unloaded filter sample both devices cover the MPPS-region around 300 nm (b). The diffusion regime below the MPPS size down into the nanometer region is completely considered by the SMPS measurement. The OPC measurement is crucial to cover the majority of the inertia-dominated part of the fractional separation efficiency curve up to a size range of 2–4 μm. However, after cake formation to (in this case) 200 Pa, only a small fraction of the inertia regime for a size range of 600 nm up to 1 μm is covered exclusively by the OPC measurement (d). For increased differential pressures the majority of the fractional separation efficiency curve can be determined from SMPS measurements alone.

The unloaded filter medium shows a very wide penetration range from approx. 10 nm at the lower end up to sizes exceeding 1 μm. Especially for these larger particles the test aerosol has significant drawbacks (low number of counting events for these size classes), as not the entire fractional separation efficiency curve can be measured up to the highest particle diameter. In this case the combination of filter medium and test aerosol does not match very well and a test aerosol with larger particle sizes would have been necessary. However. These sizes are not really relevant within the scope of this investigation for three main reasons:

- The fractional separation efficiency improves rapidly, as e.g. a differential pressure increase of 100 Pa (from 100 Pa of the medium up to 200 Pa of the loaded filter sample) is already enough to completely separate particle sizes > 1 μm. In filter testing (and operation) larger differential pressures / cake thicknesses occur (e.g. 1000 Pa as maximum differential pressure according to VDI 3926) so that the duration where larger particles can penetrate the filter medium is very short. Do note however that the penetration of these particles could significantly impact gravimetrical particle concentrations.
- For each experiment new filter samples were evaluated. An effect typically occurring for cake-forming surface filters is filter aging with ongoing filter operation across multiple filtration cycles. Under operation the filters are regenerated whereby cake detachment occurs and renewed particle penetration into the filter matrix is possible. The deposition of particulate matter in the filter matrix increases both the separation efficiency and the residual differential pressure. Here, structural changes of the filter medium significantly affect the filtration characteristics. These filter aging effects will likely narrow the penetration-relevant size range and the evaluation of new samples somewhat presents a “worst case”-scenario with the highest particle penetration.
- Other filter materials are known to be more efficient [compare e.g. (Simon et al., 2014)] and the selected material already showed comparably high dust emissions in past experiments (Bächler et al., 2026). For filter media with better separation characteristics these larger sizes will not play a role [compare e.g. (Lacerda et al., 2022)].

Nonetheless, as a consequence, only a size range below 2 μm will be discussed in the results section since the number of particles in this region is sufficiently high to determine accurate separation efficiencies. Furthermore, particle sizes below 200 nm are not considered for further evaluation in case of the OPC due to the sharp drop in counting efficiency.

2.7. *Measurements considering aerosol stability for the experimental procedure*

As already stated, there are two major requirements to correctly determine the fractional separation efficiency:

- The generated test aerosol has to be stable during the measurement duration (e.g. scanning procedure of the SMPS)
- The filtration performance has to remain constant so that filtration of the test aerosol does not contribute to cake formation and the deposition of test aerosol into the filter matrix or the dust cake does not lead to significant changes of the structural properties that may impact the filtration performance.

A direct experimental validation regarding structural properties of filter medium and dust cake was not possible within the scope of the investigation. To add further context with regards to aerosol stability on raw- and clean-gas side for the determination of the fractional separation efficiency an additional measurement was performed (Fig. 5). Due to scheduling conflicts these experiments could not be performed in the identical test rig but were performed in an equivalent test rig based on VDI 3926 with the same general setup shown in Fig. 1 (filter face velocity 2 m/min only). The particle number concentrations resulting from the generated NaCl and high-purity water aerosol were monitored for prolonged durations on the raw-gas side (CPC 3775) and clean-gas side (CPC 3756 – formerly used as detector for the SMPS-system). The aerosol spectrometer was not part of this investigation. The temporally resolved penetration behavior of the generated aerosol was measured for two different differential pressure levels (before and after cake formation). During cake formation using Pural SB as test dust the NaCl and high-purity water aerosol generation was stopped and the two CPCs were disconnected from the test rig.

On the raw-gas side there is a slight cyclical behavior of the generated aerosol, where concentrations fluctuate due to minor instabilities of the pressurized air supply network for the nebulizers. This behavior is not notable with regards to the concentrations measured on the clean-gas side where no such fluctuations are detected by the CPC. For the filter medium alone, the total separation efficiency resulting from the fluctuations in raw-gas concentration varies between approx. 0.64 and 0.72. In the context of the performed SMPS-scans these fluctuations are

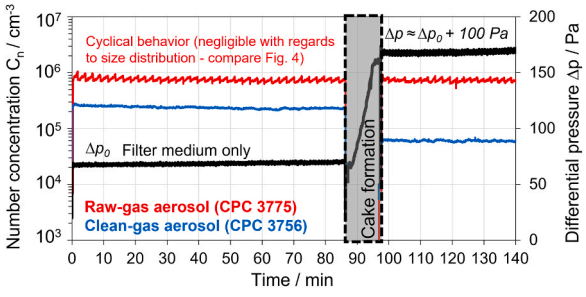

Fig. 5. Prolonged measurement of raw-and clean-gas particle concentrations during filtration of the NaCl / high purity water test aerosol for two differential pressure levels.

negligible (compare Fig. 4). Over the prolonged measurement period the particle concentration is very stable and at a sufficiently high level to determine fractional separation efficiencies across multiple orders of magnitude. The increase in separation efficiency after the formation of the dust cake is also highlighted by the measurements due to the decrease of (constant) particle penetration at the higher differential pressure (total separation efficiency between approx. 0.91 and 0.93).

Summarizing, the filtration performance is not altered due to potential structural changes of filter medium and dust cake caused by the deposition of particles from the NaCl / high purity water test aerosol. The sufficient aerosol stability on raw- and clean-gas side enables a valid determination of the fractional separation efficiency within the scope of the presented experimental methodology.

3. Results and discussion

3.1. Fractional separation efficiency of the filter medium

Over the course of the investigation multiple experimental runs were performed whereby the initial fractional separation efficiency of the filter medium (no dust cake) was determined. The results of these measurements are summarized in Fig. 6.

Comparing the individual experimental runs, there are minor differences between the individual fractional separation efficiency curves. The majority of samples [excluding one outlier (measurement 7)] has a MPPS between 180 – 300 nm at efficiencies between 0.5 up to 0.6. The outlier starts at a somewhat increased efficiency of 0.7 at a MPPS of approx. 280 nm and is thus still in a similar region The dust cake for measurement 7 was built up to a differential pressure of 500 Pa (phase 2) where (almost) no particle penetration could be detected (in phase 3) and should therefore not be the cause of any contradictory results considering further evaluations in section 3.3.

There is, as was the case for the exemplary results shown in section 2.6, also a good agreement of the overlapping region of both measurement devices. This advantage of the test aerosol enables the seamless construction of fractional separation efficiency curves.

For each experimental run a new filter sample was used. Based on know-how from industrial filter manufacturers, inhomogeneities between individual samples taken from bulk stock can occur due to the production process. Therefore, pre-screening of the used filter samples was performed for the experiments in this publication. The corresponding samples all had similar starting differential pressures (approx. 90 – 100 Pa) for the selected filter face velocity. The differences between the individual samples are expected to have only a minor impact on the characterization of the evolution of the fractional separation efficiency in phase 3 as shown by the investigation during phase 2 (section 3.2.).

3.2. Concentration decay during cake formation

Differences in fractional separation efficiency of the different samples using the test aerosol were shown in Fig. 6. In order to test the comparability between the different samples for further characterization in phase 3, the particle concentration decay (respectively the particle emission peak) was monitored during cake formation (test dust: Pural SB) for each filter sample up to the specific target differential pressure of the experimental run.

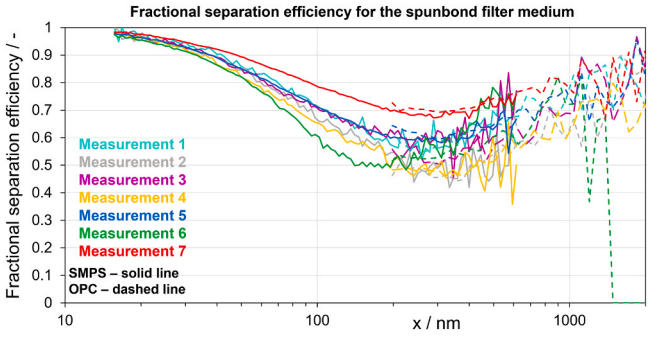

Fig. 6. Fractional separation efficiencies of the filter medium (phase 1) for multiple experimental runs each using a new filter sample.

In Fig. 7a summary of the particle concentration decay on the clean gas side for all experimental runs is displayed considering the measured particle number concentrations by the CPC (a) and OPC [(b) and (c)]. In case of the OPC, the particle size distributions for the corresponding size range of 200 nm up to 10 µm were evaluated for the individual runs to estimate the contribution of supermicron particles to the total particle emission for sizes that were not covered by the test aerosol (compare Fig. 4). Here, the size distribution shortly after passing the maximum concentration of the emission peak and right before reaching the target differential pressure are plotted for the individual experiments.

The agreement of the particle concentration decay on the clean-gas side is very good for all individual runs for both aerosol measurement devices. There is a precise overlap of the corresponding decay curves even though there were deviations between the individual fractional separation efficiency curves (Fig. 6). This behavior is likely linked to the size distribution of the test dust (coarse dust – only small amount of nanoparticles) and the fast cake formation. Note that when reaching the target differential pressure, the concentration drops rapidly as dust dosage and cake formation are stopped. Concentration decay proceeds faster in case of the OPC measurement, as the MPPS region narrows down during cake formation and particles below the detectable size range of the OPC make up a larger fraction of the resulting particle emission. Thus, the penetration of MPPS-relevant (nano-) particles contributes significantly to the total particle emission. The size distribution obtained from OPC measurements gives a clear indication of the change of penetration-relevant size range. While at the height of the emission peak particles larger than 1 µm diameter can penetrate the filter medium (and the corresponding thin dust cake), after a short increase in cake thickness (here: 50 Pa increase in differential pressure) only submicron particles of the test dust can penetrate to the clean gas side. This adds further context to the selection of the test aerosol that was constricted regarding an upper particle diameter of “only” 2 µm, as particles exceeding this size do not play a significant role in the context of a filtration process including filter aging and prolonged (multiple) filtration cycles. The NaCl aerosol has a sufficient size range for an in-depth characterization of the evolution of the fractional separation efficiency.

3.3. Evolution of the fractional separation efficiency with proceeding cake formation

After discussing the fractional separation efficiency of the filter medium and the particle concentration decay during cake formation, the evolution of the fractional separation efficiency with proceeding cake formation is discussed (phase 3 of the experimental methodology). In Fig. 8 the average fractional separation efficiency of the filter medium (mean of all experimental runs in Fig. 6) is compared to the fractional separation efficiency for the different target differential pressures / dust area loads of deposited dust cakes. The dust area load was determined from the known raw-gas concentration, volume flow and the duration until reaching the corresponding target differential pressure (based on the signal of the photometric measurement – compare Equation 2).

The most penetrating particle size shifts to lower particle sizes and the fractional separation efficiency at the MPPS increases with cake formation. The agreement between the fractional separation efficiencies determined from OPC and SMPS measurements in the overlapping region is again very remarkable. After a differential pressure increase of approx. 100 Pa (from 100 Pa of the filter medium to 200 Pa) the MPPS is slightly below the detectable size range of the OPC. At this point the entire penetration-relevant size range can be measured with the SMPS-

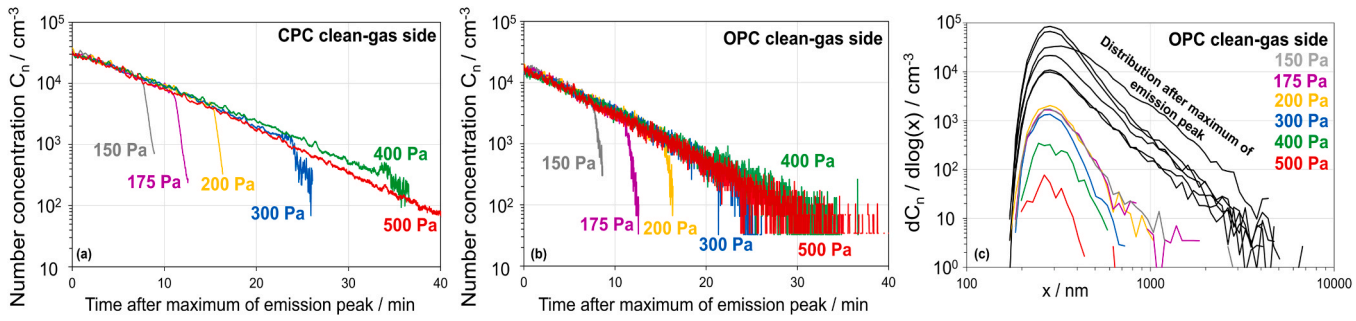

Fig. 7. Particle concentration decay during cake formation (phase 2) of the experiments. Total particle number concentration measured by a CPC (a); particle number concentration (b) and particle size distribution (c) measured by an OPC (measurement range approx. 200 nm – 10 µm).

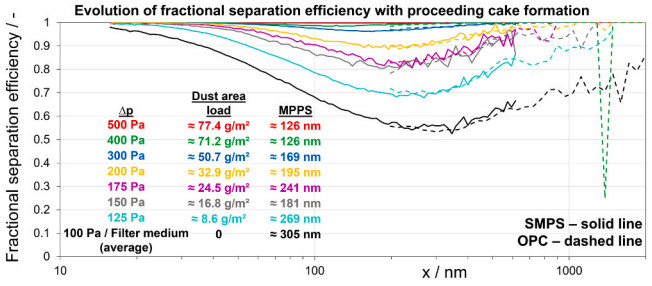

Fig. 8. Evolution of the fractional separation efficiency with proceeding cake formation (phase 3) as a function of differential pressure / dust area load of the filter cake.

system alone. Further increasing the cake thickness leads to very high separation minima close to unity. E.g. for 400 Pa differential pressure the fractional separation efficiency is larger than 0.98 at the MPPS (Fig. 9). At 500 Pa the minimum efficiency is larger than 0.998.

Fig. 10 shows further evaluations of the fractional separation efficiency curves from Fig. 9. The minimum efficiency at the MPPS, MPPS particle size and an average separation efficiency are plotted as a function of dust area load of the filter medium (a). The average separation efficiency was related to an upper size of approx. 4 µm to match an upper emission-relevant particle size from the fractional separation efficiency curves (Fig. 6) and data from OPC-measurements during cake formation (Fig. 7). For further context the correlation between dust area load and differential pressure for the experiments is also shown in Fig. 10 (b).

The MPPS size decreases from approx. 300 nm down to just above 100 nm. At this point almost no particle penetration can be measured. Here, the surface filter behaves like an "ideal" separator ($T(x) = const. = 1$). The starting efficiency of the filter material is not remarkably high (e.g. compared to HEPA-filters) but cake formation rapidly closes the separation gap, especially considering the average separation efficiency.

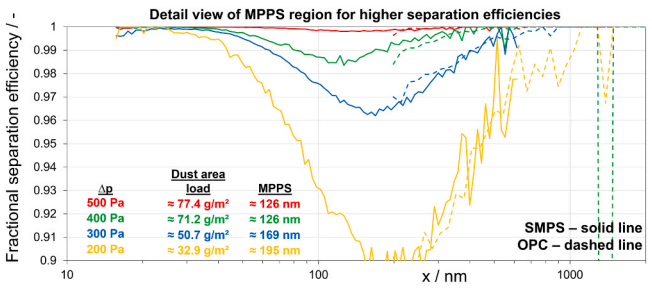

Fig. 9. Evolution of the fractional separation efficiency with proceeding cake formation (phase 3) as a function of differential pressure / dust area load of the filter cake (detail view).

A brief explanation on the observed trends, considering shift in MPPS and increase in fractional separation efficiency can be found in sect. 3.3.1.

The results have implications for filter operation, as even for comparably low differential pressures (here: 500 Pa) remarkable fractional separation efficiencies are reached. Prolonging the filtration cycle further can significantly lower the (average) dust emission while filter regeneration (and cake detachment) would cause a renewed particle penetration according to the determined filtration kinetics. The results demonstrate that submicron particles and nanoparticles dominate the particle emission for cake-forming surface filters in gas cleaning applications. While this information is not inherently new it has never been quantitatively analyzed for the entire submicron and nanoscale size range. This means that sophisticated measurements using suitable measurement devices (dependent on the expected size range of the particle emission according to the handled raw-gas aerosol) are necessary to accurately characterize particle emissions. Within current limits for these filters in the industrial application, only gravimetrical measurements are considered where the contribution of these sizes is negligible. The results also show that a single "Most-Penetrating-Particle-Size" does not exist for cake-forming surface filters, rather the MPPS during operation depends on the actual loading state / deposited dust mass on the filter medium.

3.3.1. A brief theoretical discussion of particle separation during caking forming filtration using the classical filtration theory

As was shown in section 3.3 an increase in dust area load is linked to an increase in fractional separation efficiency across the entire particle size range and a decrease of the most-penetrating particle size. In this section the experimental results are put into context of the classical filtration theory.

In general, the penetration or fractional separation efficiency of particles with a certain size x through a clean filter medium (or any form of filtering structure such as porous materials, filter cakes, etc.) can be calculated from single-fiber collection efficiency and the structural parameter of the given filter medium according to Equations 4 and 5.

$$P(x) = \exp\{-\eta(x) \bullet f\} \quad \text{Eq. 4}$$

$$T(x) = 1 - P(x) = 1 - \exp\{-\eta(x) \bullet f\} \quad \text{Eq. 5}$$

If particle separation is predominantly driven by the diffusion and interception mechanism, as is the case for most of the penetrating particles around the MPPS region in this investigation, the resulting particle separation can be expressed as a series connection of the two mechanisms (Equation 6, compare Lee and Liu, 1982)

$$P(x) = \exp\{-[a \bullet \eta_D(x) + b \bullet \eta_I(x)] \bullet f\} \quad \text{Eq. 6}$$

Both mechanisms interact with particle size, whereby an increase in particle size leads to a decrease of single fiber collection efficiency based on diffusion (Equation 7) and an increase of single fiber collection efficiency based on interception (Equation 8).

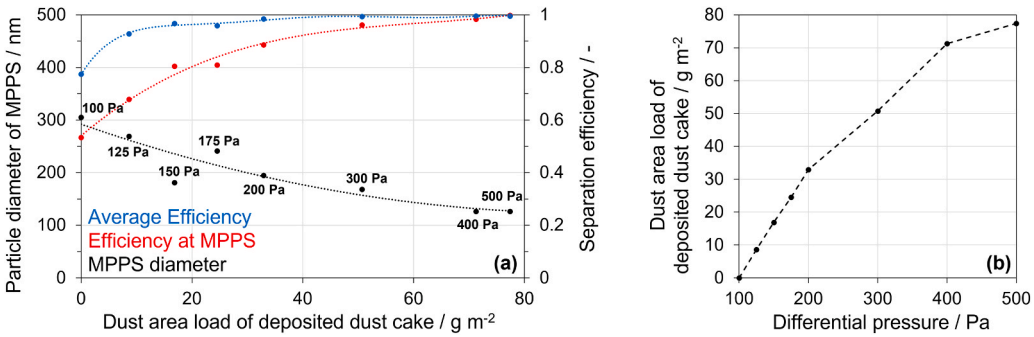

Fig. 10. Evolution of MPPS size and fractional separation efficiencies with increasing dust area load of separated dust cake (a) and correlation between differential pressure and dust area load of deposited dust cake (b).

$\eta_D(x) \searrow for\ x \nearrow$ Eq. 7

$\eta_I(x) \nearrow for\ x \nearrow$ Eq. 8

If particle separation is dominated by diffusion $a \bullet \eta_D(x) \gg b \bullet \eta_I(x)$, respectively

$a \bullet \eta_D(x) \ll b \bullet \eta_I(x)$ if particle separation is dominated by the interception mechanism. For filtration applications, the size range where $a \bullet \eta_D(x) \approx b \bullet \eta_I(x)$ is of special interest due to comparably low resulting fractional separation efficiencies. In many cases of aerosol filtration this size range is approx. 100 – 600 nm dependent on the structural properties of the filter medium and on the filtration conditions. In any case, a minimum efficiency min $[a \bullet \eta_D(x) + b \bullet \eta_I(x)]$ can be determined at a corresponding most penetration particle size x_{MPPS}. The interaction between particle size and diffusion and interception mechanism is known as "diffusion-interception trade-off".

In case of cake-forming surface filtration, the resulting particle penetration efficiency for particles of size x can, in a simplified approach, be calculated as a series connection of filter medium and dust cake. Due to the growth of dust cake, the penetration efficiency depends on the filtration time. Here, filtration time respectively the separated dust area load can significantly affect the particle separation.

$$P(x,t) = \exp\{-\eta_{FM}(x) \bullet f_{FM}\} \bullet \exp\{-\eta_{DC}(x) \bullet f_{DC}(t)\} \quad \text{Eq. 9}$$

Assuming ideal cake-forming surface filtration, the dust area load (as a measure of cake thickness and separation characteristics) increases proportional to the amount of separated dust over the course of the filtration time on the filter medium. The structural properties of the dust cake itself (i.e. porosity / packing density) are independent of dust area load and are assumed to remain constant. Under constant filtration conditions, Equation 10 can be applied.

$$f_{DC}(t) = c_0 \bullet t \quad \text{Eq. 10}$$

For the other parameters in Equation 9, Eq.11–13 hold true during ideal continuous cake-forming filtration.

$$\eta_{FM}(x) = const. \quad \text{Eq. 11}$$

$$f_{FM} = const. \quad \text{Eq. 12}$$

$$\eta_{DC}(x) = const. \quad \text{Eq. 13}$$

Thus, the fractional separation efficiency always increases for any particle size x during cake formation with an increase in filtration time $[P(x, t > 0) < P(x, t = 0)]$. This is clearly shown, for example, by the measurement results in Fig. 8.

Furthermore, the separation efficiency of the dust cake is also influenced by the diffusion-interception trade-off. The particle separation through the dust cake is mainly affected by an improvement of the contribution of the interception mechanism and more significantly affects larger particle sizes. In case that the interception the dominate separation mechanism for the particle size x, Eq. 14 holds true.

$$\eta_{DC}(x_1) < \eta_{DC}(x_2) \ \text{ for } \ x_1 < x_2 \quad (14)$$

For further analysis, Equation 9 can be rearranged.

$$P(x,t) = C_1 \bullet \exp\{-\eta_{DC}(x) \bullet c_0 \bullet t\} \quad \text{Eq. 15}$$

As the separation characteristics of the filter medium remain constant, linearizing Equation 15 yields the filtration kinetics (Equation 16) of a certain particle size x similar to the concentration decay curves shown in Fig. 7

$$\log[P(x,t)] = C_2 - \eta_{DC}(x) \bullet c_0 \bullet t \quad \text{Eq. 16}$$

Therefore, for any particle size x, $\log[P(x,t)]$ decreases linearly with increase in filtration time under constant filtration conditions. For the case $x_1 < x_2$, the decrease of $\log[P(x_2,t)]$ proceeds faster than $\log[P(x_1,t)]$ due to a higher single-fiber collection efficiency that is mainly based off the interception mechanism. This also holds true for the comparison of OPC and CPC particle concentration data shown in Fig. 7 (faster decrease for the larger particle sizes that are within the measurement range of the OPC). Due to this behavior the most penetration particle size is shifting towards smaller particle sizes with increasing filtration time. This shift of MPPS causes an increasing relevance of diffusional particle separation for the corresponding MPPS at the filtration time t. That means, diffusion is playing an increasingly significant role in the contribution to the resulting single-collector separation efficiency $\eta_{DC}(x_{mpps}(t))$. This leads to the theoretical conclusion that the shift of the MPPS towards smaller particle sizes will ultimately reach a limit after a certain filtration time. This is illustrated by the evaluation results shown in Fig. 10, where the change in MPPS decreases and seems to approach a constant particle size.

3.4. Concluding considerations on the experimental methodology

The experimental methodology and the selection of the test aerosol were suitable for characterizing the evolution of the fractional separation efficiency for cake-forming surface filters. There was a good agreement between OPC and SMPS measurements. Here, for both measurement systems the ratio of raw- and clean-gas particle concentration in the overlapping measurement region corresponded very well and resulted in almost identical fractional separation efficiencies, additionally the actual absolute concentrations were in many cases also identical between the devices for a corresponding size class. In practical applications, the good agreement between optical and electrical mobility diameter does not require a sophisticated calibration (compare e.g. Binnig et al., 2007) for the selected test aerosol. The emission relevant size range was mostly covered, except for cases with little (or no) deposited dust cake where the penetration range exceeded the size distribution of the test dust. By adjusting the concentration of the salt solution for the corresponding nebulizers, this size range could be shifted to larger particle sizes to better cover the complete emission relevant

size-range at the beginning of the filtration process.

Typical test dusts that are conventionally used in filter testing may not cover the entire emission-relevant size range, especially the nanometer-region. Furthermore, different test aerosols might create larger disagreements between electrical mobility and optical particle diameter. This was e.g. observed for the used test dust Pural SB in this study (Fig. 2). Thus, the selected NaCl solution turned out to be a suitable choice.

Both, raw-gas and clean-gas particle concentrations were constant during the characterization phases of the fractional separation efficiency. Due to the short measurement durations, stability of the test aerosol on the raw-gas side was not an issue. For longer measurement durations (e.g. clean-gas measurement and scans across multiple filtration cycles) the raw-gas aerosol stability should be checked regularly during the cycle (e.g. before filter regeneration). Considering particle emissions, no change in separation efficiency during SMPS scans was noticed (based on continuous monitoring of clean-gas particle concentrations) so that suitable measurement conditions for the SMPS system could be realized. For more efficient filter media or other types of dust, where cake formation proceeds at a faster pace or more compact dust cakes are formed, the test aerosol could potentially contribute to cake formation. In these cases, the measurement methodology would have to be adapted (e.g. shorter scan durations or post-processing of SMPS data). Approaches to correct SMPS measurements for decaying particle concentration are reported in (Bächler et al., 2024).

For higher separation efficiencies (and at the upper and lower end of the size distribution of the test aerosol) only a limited number of (e.g. single digit or even zero) counting events can be detected on the clean-gas side in a certain measurement interval. This can limit the resolution of the fractional separation efficiency and may lead to high fluctuations for particle sizes that can still penetrate to the clean-gas side [$T(x) < 1$] but already occur in low concentrations on the raw-gas side. As already stated, to avoid this problem the size distribution of the test aerosol should be as broad as possible and exceed the size range of the fractional separation efficiency curve. A solution to further improve the resolution, for these cases with high fractional separation efficiencies or a low number of counting events, the measurement intervals (e.g. scan duration) could be enhanced to increase the absolute number of counting events on the clean-gas side and the statistical significance of the concentration measurement for an individual scan. Due to the shown behavior of the fractional separation efficiency curve (Fig. 8), the time of the measurement intervals could be changed dependent on the corresponding dust area load on the filter medium.

For the new filter sample or low dust area loads, shorter measurement intervals are sufficient, as the majority of the particle emission occurs at the beginning of the filtration cycle (emission peak), where sufficient number of counting events enable an accurate determination. This also includes the larger particle sizes that contribute the most to gravimetrical dust emissions. With increase in filter loading, the time for the measurement intervals could be dynamically increased to enable a more accurate determination for higher separation efficiencies where the number of counting events in a certain measurement interval is limited.

In the context of praxis-relevant filter testing the adaptation of the shown methodology into test procedures is unlikely due to the high measurement effort. Even though aerosol spectrometers are limited by the lower detection limit of approx. 200 nm and cannot measure the entire fractional separation efficiency curve, they are still a suitable device to characterize the majority of the (submicron fine-) dust particle emission, especially when resorting to (gravimetrical) $PM_{2.5}$ concentrations. At the beginning of a filtration cycle most of the MPPS-region (e.g. beyond the minimum efficiency at approx. 300 nm) is covered by OPC measurements. It of course strongly depends on the handled dust and its size distribution whether a suitable measurement of the particle emission applying aerosol spectrometers is possible. For cases where the separation efficiency improves rapidly and barely overlaps with the measurement region of the OPC (e.g. membrane filter media), the majority of the particle emission may remain undetected. This has also been shown in praxis-relevant measurements where only a small and temporal overlap between handled aerosol (ash & soot) and membrane filter media with the measurement region of an OPC resulted in very short emission peaks (Bächler et al., 2026 and 2024). For most dusts used in filter testing this should not be an issue due to a significant amount of larger particles ($x >> 1$ µm). Therefore, the integration of these devices into filter test procedures is recommended due to comparably simple handling and a more accurate determination of particle emissions (e.g. temporally resolved measurement) in the context of the actual separation characteristics of the filter media.

Other devices that were not used in this study (such as EEPS or ELPI) will be considered for further measurements to offer additional context and exploit the advantages of the individual measurement device as best as possible.

4. Summary and outlook

The evolution of the fractional separation efficiency for cake-forming surface filter media for gas cleaning applications was characterized in a filter test rig. Adequate aerosol measurement technology (OPC, CPC, SMPS-system) that spans the emission-relevant size range (from approx. 10 nm – 2 µm) was applied. A dedicated experimental methodology including measurement phases for characterization of the fractional separation efficiency using test aerosols with a wide submicron and nanoscale size distribution (dried NaCl & high-purity water aerosol) and a phase for cake formation using a test dust (Pural SB) was developed and applied for multiple experimental runs and filter media samples. The corresponding test aerosol covered (almost) the entire emission-relevant size range. Significant attention was paid to the fact that the test aerosol may not contribute to cake formation and an improvement of the separation efficiency as to not influence SMPS scans due to a fast concentration decay.

Small increases in differential pressure (e.g. from 100 Pa of the filter medium up to 200 Pa of filter medium and dust cake) significantly increase the minimum separation efficiency (for the aforementioned example from 53.3% to 88.6%) and cause a decrease in most penetrating particle size (for the aforementioned example from 305 nm to 169 nm). At this point the fractional separation efficiency can completely be determined from SMPS measurements, where before the combination of the different measurements devices (OPC and SMPS-system) was necessary. There was a very good agreement in the overlapping region of the size ranges of the measurement devices regarding the determined fractional separation efficiencies (different measurement principles: electrical mobility analysis vs. scattered light based detection). The change of the fractional separation efficiency curves and shrinking of the separation gap highlights the relevance of submicron and nanoparticles in the context of dust emissions where (until now) only gravimetrical measurements are mandatory for industrial limits and filter testing standards. At a differential pressures of 400 – 500 Pa almost no particle penetration can be measured even in the nanoscale size region.

This investigation laid the groundwork for future research. The filter medium was an exemplary spunbond filter medium with a comparably low separation efficiency. Different filter materials can be investigated applying the experimental methodology but might require modifications dependent on the separation properties and surface treatment (e.g. membrane filter media that significantly promote cake formation). Different (praxis-relevant) test dusts can be used to estimate filter performance and the penetration of submicron and nanoscale aerosols under more realistic conditions compared to conventionally used test dusts. Furthermore, in-depth modeling of particle emissions where the filter medium and growing dust cake influence the fractional separation efficiency can be performed based on the results. In a next step in research additional materials and the effect of filter regeneration and filter aging on the fractional separation efficiency and its evolution will

be evaluated. Further approaches will aim to adapt the experimental methodology that, so far, has been an “offline” procedure, to an “online” procedure that enables the characterization of the fractional separation efficiency during filter operation across multiple filtration cycles and thus facilitate the inclusion into the conventional operation of filter test rigs and standards.

CRediT authorship contribution statement

Peter Bächler: Writing – original draft, Methodology, Investigation, Data curation, Conceptualization. **Felizia Zhang:** Writing – review & editing, Investigation, Data curation. **Jörg Meyer:** Writing – review & editing, Validation, Methodology, Conceptualization. **Qian Zhang:** Writing – review & editing, Validation, Methodology, Conceptualization. **Achim Dittler:** Writing – review & editing, Resources, Conceptualization.

Declaration of Generative AI and AI-assisted technologies in the writing process

During the preparation of this work the authors did not use any generative AI and AI-assisted technologies.

Declaration of Competing Interest

The authors declare that they have no known competing financial interests or personal relationships that could have appeared to influence the work reported in this paper.

Data availability

Data available on request from the authors. The data that support the findings of this study are available from the corresponding author upon reasonable request.

References

Bach, B., Schmidt, E., 2007. Influence of leaks in surface filters on particulate emissions. J. Hazard. Mater. 144 (3), 673–676. https://doi.org/10.1016/j.jhazmat.2007.01.093.

Bächler, P., Meyer, J., Dittler, A., 2022. Measurement of transient nanoparticle emissions of pulse-jet cleaned filters applying an engine exhaust particle sizer. Aerosol Sci. Technol. 56 (4), 394–402. https://doi.org/10.1080/02786826.2022.2027335.

Bächler, P., Meyer, J., Dittler, As, 2023. Spatially resolved online leak detection in a baghouse filter applying low-cost PM-Sensors. Chem. Ing. Tech. 95 (1-2), 178–188. https://doi.org/10.1002/cite.202200116.

Bächler, P., Meyer, J., Dittler, A., 2026. Implications for the energy-evaluation of pulse-jet cleaned surface filter media regarding filter operation during typical test procedures. Powder Technol. 469, 121889. https://doi.org/10.1016/j.powtec.2025.121889.

Bächler, P., Meyer, J., Ligotski, R., Krug, P., Dittler, A., 2024. Measurement of transient nanoparticle emissions of a municipal biomass incineration plant equipped with pulse-jet cleaned filters. Process. Saf. Environ. Prot. 184, 601–614. https://doi.org/10.1016/j.psep.2024.02.013.

Binnig, J., Meyer, J., Kasper, G., 2007. Calibration of an optical particle counter to provide mass for well-defined particle materials. J. Aerosol Sci. 38 (3), 325–332. https://doi.org/10.1016/j.jaerosci.2006.12.001.

Binnig, J., Meyer, J., Kasper, G., 2009. Origin and mechanisms of dust emission from pulse-jet cleaned filter media. Powder Technol. 189 (1), 108–114. https://doi.org/10.1016/j.powtec.2008.06.012.

Boudhan, R., Joubert, A., Gueraoui, K., Durécu, S., Venditti, D., Tran, D.T., Le Coq, L., 2018. Pulse-jet bag filter performances for treatment of submicronic and nanosized particles from waste incineration. Waste Biomass-.-. Valor 9 (5), 731–737. https://doi.org/10.1007/s12649-017-9858-4.

DIN EN ISO 16890: Air quality – Air Filters for General Ventilation—Part 1: Technical Specifications, Requirements and Classification System Based upon Particulate Matter Efficiency (ePM)(ISO 16890-1: 2016), Standard, Berlin, Beuth Verlag GmbH.

DIN ISO 11057: Air quality – Test method for filtration characterization of cleanable filter media (ISO 11057:2011), Standard, Berlin, Beuth Verlag GmbH.

Ding, Y., Cai, F., Fan, C., Zhou, G., Zhang, D., Shang, Q., Zhang, F., Zhong, Z., Xing, W., 2025. Effects of ammonium sulfates and relative humidity on filter cake structure and filtration resistance of baghouse. J. Environ. Chem. Eng. 13 (5), 118661. https://doi.org/10.1016/j.jece.2025.118661.

European Commission, (2020). Regulation (EC) No 715/2007 of the European Parliament and of the Council of 20 June 2007 on type approval of motor vehicles with respect to emissions from light passenger and commercial vehicles.

European Commission, Joint Research Centre, Daginnus, K., Marty, T., Trotta, N.V., Brinkmann, T., Whitfield, A., Roudier, S., 2023. Best available techniques (BAT) reference document for common waste gas management and treatment systems in the chemical sector – Industrial Emissions Directive 2010/75/EU (integrated pollution prevention and control). Publications Office of the European Union, DOI: 10.2760/220326.

European Union: Directive (EU) 2024/2881 of the European Parliament and of the Council of 23 October 2024 on ambient air quality and cleaner air for Europe (recast), https://eur-lex.europa.eu/eli/dir/2024/2881/oj (last access: 7 August 2025).

Hoeflinger, W., 2025. PM2.5 separation efficiency and energy assessment for cleanable dust- and oil-water soluble mist filter media. Process. Saf. Environ. Prot. 197, 106950. https://doi.org/10.1016/j.psep.2025.106950.

Khirouni, N., Charvet, A., Thomas, D., Bémer, D., 2020. Regeneration of dust filters challenged with metallic nanoparticles: influence of atmospheric aging. Process. Saf. Environ. Prot. 138, 1–8. https://doi.org/10.1016/j.psep.2020.02.040.

Knisley, J.P., Meyer, J., Dittler, A., 2026. Methodology for the characterization of pleated filter media in a pulse-jet-cleaned test-rig in accordance to DIN ISO 11057. Sep. Purif. Technol. 389, 136720. https://doi.org/10.1016/j.seppur.2025.136720.

Kurtz, O., Meyer, J., Kasper, G., 2016. Influence of filter operating parameters on fine dust emissions from pulse-cleaned filter bags. Chem. Eng. & Technol. 39 (3), 435–443. https://doi.org/10.1002/ceat.201500340.

Kurtz, O., Meyer, J., Kasper, G., 2017. The contribution of small leaks in a baghouse filter to dust emission in the PM2.5 range—a system approach. Particuology 30, 40–52. https://doi.org/10.1016/j.partic.2016.08.001.

Lacerda, C.R. de, Bächler, P., Schwarz, A.D., Sartim, R., Aguiar, M.L., Dittler, A., 2022. Impact of seams on the operating behavior of surface filters regarding particle emissions. Chem. Eng. & Technol. 45 (7), 1354–1362. https://doi.org/10.1002/ceat.202200132.

Lee, K.W., Liu, B.Y.H., 1982. Theoretical study of aerosol filtration by fibrous filters. Aerosol Sci. Technol. 1 (2), 147–161. https://doi.org/10.1080/02786828208958584.

Leung, W.W.-F., Choy, H.-F., 2018. Transition from depth-to-surface filtration for a high-efficiency, high-skin effect, nanofiber filter under continuous nano-aerosol loading. Chem. Eng. Sci. 182, 67–76. https://doi.org/10.1016/j.ces.2018.02.024.

Li, J., Wu, Q., Huang, Y., Sun, Z., Li, J., Wu, D., 2022. Particulate matters filtration by a filter medium with pin holes: modeling and experimental verification. Process. Saf. Environ. Prot. 158, 282–290. https://doi.org/10.1016/j.psep.2021.12.012.

Schiller, S., Schmid, H.-J., 2015. Highly efficient filtration of ultrafine dust in baghouse filters using precoat materials. Powder Technol. 279, 96–105. https://doi.org/10.1016/j.powtec.2015.03.048.

Simon, X., Bémer, D., Chazelet, S., Thomas, D., 2014. Downstream particle puffs emitted during pulse-jet cleaning of a baghouse wood dust collector: Influence of operating conditions and filter surface treatment. Powder Technol. 261, 61–70. https://doi.org/10.1016/j.powtec.2014.04.028.

Steiner, D., Lanzerstorfer, C., 2024. Particulate emissions from biomass power plants: a practical review and measurement uncertainty issues. Clean. Techn Environ. Policy 26 (4), 1039–1048. https://doi.org/10.1007/s10098-023-02645-6.

VDI 3926, Part 1: Testing of cleanable filter media – Standard test for the evaluation of cleanable filter media, Guideline, Berlin, Beuth Verlag GmbH, 2004.

Zhang, Q., 2022. Online-Partikelmessung im Reingas zu Beginn der kuchenbildenden Staubabscheidung mit Nadelfilzen in der Gasreinigung. Chem. Ing. Tech. 94 (4), 572–584. https://doi.org/10.1002/cite.202100053.